Temporal analysis of grating formation in photopolymer using the nonlocal polymerization-driven diffusion model

John V. Kelly, Michael R. Gleeson, Ciara E. Close, Feidhlim T. O' Neill, John T. Sheridan

Department of Electronic and Electrical Engineering, Faculty of Engineering and Architecture, University College Dublin, Belfield, Dublin 4, Ireland
john.sheridan@ucd.ie

Sergi Gallego, Cristian Neipp

Departamento de Física, Ingeniería de Sistemas y Teoría de la Señal, Departamento Interuniversitario de Óptica, Universidad de Alicante, Apartado 99, E-03080 Alicante, Spain

Abstract: The nonlocal polymerization-driven diffusion model (NPDD) has been shown to predict high spatial frequency cut-off in photopolymers and to accurately predict higher order grating components. We propose an extension to the NPDD model to account for the temporal response associated with polymer chain growth. An exponential response function is proposed to describe transient effects during the polymerization process. The extended model is then solved using a finite element technique and the nature of grating evolution examined in the case when illumination is stopped prior to the saturation of the grating recording process. Based on independently determined refractive index measurements we determine the temporal evolution of the refractive index modulation and the resulting diffraction efficiency using rigorous coupled wave theory. Material parameters are then extracted based on fits to experimental data for non-linear and both ideal and non-ideal kinetic models.

OCIS codes: (050.7330) Volume holographic gratings; (090.2900) Holographic recording materials; (090.2890) Holographic optical elements.

References and links

1. S. Schultz, E. Glytsis, T. Gaylord, "Design, Fabrication, and Performance of Preferential-Order Volume Grating Waveguide Couplers," Appl. Opt. **39**, 1223-1232 (2000).
2. L. Dahr, A, Hale, K. Kurtis, M. Schnoes, M. Tackitt, W. Wilson, A. Hill, M. Schilling, H. Katz, A. Olsen, "Photopolymer Recording Media for High Density Data Storage," in *Proceedings of IEEE conference on Optical Data Storage* Conference (Institute of Electrical and Electronics Engineers, Canada, 2000) pp. 158-160.
3. J. T. Sheridan, F. T. O' Neill, J. V. Kelly, "Holographic Data Storage: Optimized Scheduling using the Non-local Polymerization Driven Diffusion Model," J. Opt. Soc. Am. B **21**, 1443-1451 (2004).
4. J. R. Lawrence, F. T. O'Neill, "Photopolymer holographic recording material," Optik (The International Journal for Light and Electron Optics) **112**, 449-463 (2001).
5. G. Zhao, P. Mouroulis, "Diffusion model of hologram formation in dry photopolymer materials," J. Mod. Opt. **41**, 1929-1939 (1994).
6. J. T. Sheridan, J. R. Lawrence, "Non-local response diffusion model of holographic recording in photopolymer," J. Opt. Soc. Am. A **17**, 1108-1114 (2000).
7. J. H. Kwon, H. C. Chang, K. C. Woo, "Analysis of temporal behavior of beams diffracted by volume gratings formed in photopolymers," J. Opt. Soc. Am. B **16**, 1651-1657 (1999).
8. G. Odian, *Principles of Polymerization* (Wiley, New York, 1991).
9. J. R. Lawrence, F. T. O'Neill, J. T. Sheridan, "Adjusted intensity nonlocal diffusion model of photopolymer grating formation," J. Opt. Soc. Am. B **19**, 621-624 (2002).

10. J. V. Kelly, F. T. O'Neill, J. T. Sheridan, C. Neipp, S. Gallego, M. Ortuno, "Holographic photopolymer materials: non-local polymerisation driven diffusion under non-ideal kinetic conditions," J. Opt. Soc. Am. B **22**, 407-416 (2005).
11. S. Blaya, L. Carretero, R. F. Madrigal, M. Ulibarrena, P. Acebal, A. Fimia, "Photopolymerization model for holographic gratings formation in photopolymers," Appl. Phys. B 77, 639-662 (2003).
12. S. Massenot, J.-L. Kaiser, R. Chevallier, Y. Renotte, "Study of the Dynamic Formation of Transmission Gratings Recorded in Photopolymers and Holographic Polymer-Dispersed Liquid Crystals," Appl. Opt. **43**, 5489-5497 (2004).
13. R. L. Sutherland, V. P. Tondiglia, L. V. Natarajan, and T. J. Bunning, "Phenomenological model of anisotropic volume hologram formation in liquid- crystal-photopolymer mixtures," J. Appl. Phys. **96**, 951-965 (2004).
14. S. Gallego, M. Ortuño, C. Neipp, A. Márquez, A. Beléndez, I. Pascual, J. V. Kelly, J. T. Sheridan, "Physical and effective optical thickness of holographic diffraction gratings recorded in photopolymers," Opt. Express **13** 1939 (2005)
15. S. Gallego, M. Ortuño, C. Neipp, A. Márquez, A. Beléndez, I. Pascual, J. V. Kelly, J. T. Sheridan, "3 Dimensional analysis of holographic photopolymers based memories," Opt. Express **13** 3543 (2005)
16. S.-D. Wu, E. Glytsis, "Holographic grating formation in photopolymers: analysis and experimental results based on a nonlocal diffusion model and rigorous coupled-wave analysis," J. Opt. Soc. Am. B **20**, 1177-1188 (2003).
17. I. Aubrecht, M. Miller, I. Koudela, "Recording of holographic gratings in photopolymers: theoretical modelling and real-time monitoring of grating growth," J. Mod. Opt. **45**, 1465-1477 (1998).
18. M. G. Moharam, T.K. Gaylord, "Rigorous Coupled-Wave analysis of planar-grating diffraction," J. Opt. Soc. Am. **71**, 811-818 (1981).
19. J. T. Sheridan, J. V. Kelly, G. O'Brien, M. R. Gleeson, F. T. O'Neill, "Generalized non-local responses and higher harmonic retention in non-local polymerization driven diffusion model based simulations," J. Opt. A: Pure Appl. Opt. **6** 1089-1096 (2004)
20. F. T. O'Neill, I. C. Rowsome, A. J. Carr, S. M. Daniels, M. R. Gleeson, J. V. Kelly, J. R. Lawrence, J. T. Sheridan, "Photo-embossed optical elements and microfluidic lens fabrication", *in Photonic Engineering*, T. J. Glynn, ed., Proc. SPIE **5827,**. (2005).
21. C. Dixon, *Numerical Analysis*, Blackie, (Glasgow and London, 1982).
22. V. L. Colvin, R. G. Larson, A. L. Harris, M. L. Schilling, "Quantitative model of volume hologram formation in photopolymers," J. Appl. Phys. **81**, 5913-5923 (1997).
23. Metricon Corporation, http://www.metricon.com/appli5.htm#anchor480218.
24. J. V. Kelly, M. R. Gleeson, F. T. O'Neill, J. T. Sheridan, C. Neipp, S. Gallego, M. Ortuno, "Examination of the temporal and kinetic effects in acrylamide based photopolymer using the nonlocal polymer driven diffusion model (NPDD)," *in Materials for Holographic and Optical Data Storage*, V. Toal, ed., Proc SPIE, Holo 05,Bulgaria, (2005).
25. http://chemfinder.cambridgesoft.com.
26. Sigma Aldrich, http://www.sigmaaldrich.com.
27. Kirk-Otmer, *Encyclopedia of Chemical Technology*, Vol. 1, (Wiley, New York, 1991).
28. F. T. O'Neill, J. R. Lawrence, J. T. Sheridan, "Automated recording and testing of holographic optical element arrays," Optik **111**,459-467 (2000).
29. M. R. Gleeson, J. V. Kelly, C. E. Close, F. T. O'Neill, J. T. Sheridan, "The Impact of Inhibition Processes during Grating Formation in Photopolymer Materials", *in Photonic Engineering*, R. F. O'Dowd, ed., Proc. SPIE **5827**, (2005).
30. A.V.Galstyan, R. S. Hakobyan, S. H, T.Galstian, "Study of the inhibition period prior to the holographic grating formation in liquid crystal photopolymerizable materials" http://www.elc.org/Documents/T.__V_Galstian_2004_05_05_11_13_17.pdf
31. The Mathworks, Inc., "Matlab 6.1," http://www.mathworks.com.
32. J. Lougnot, P. Jost and L. Lavielle, "Polymers for holographic recording: VI. Some Basic ideas for modelling the Kinetics of the recording process," Pure and Applied Optics **6**, 225-245 (1997).
33. S. Gallego, C. Neipp, M. Ortuño, A. Márquez, A. Beléndez, I. Pascual "Diffusion based model to predict the conservation of holographic gratings recorded in PVA/Acrylamide photopolymer," Appl. Opt. **42**, 5839-5845 (2003).

1. Introduction

Photopolymers have many applications ranging from integrated optical waveguide fabrication [1] to holographic data storage media [2,3]. Their versatility, ease of use and self-processing ability give them many advantages over more traditional materials such as silver halide and DCG [4]. Integral to photopolymer development is the availability of mathematical models, which accurately describe material behavior. Many such models have been proposed. Zhao and Mouroulis [5] proposed a model, which described the evolution of grating formation in

photopolymer using a four harmonic expansion of the standard 1-D diffusion equation. Sheridan et *al*. developed the Nonlocal Polymerization-Driven Diffusion (NPDD) model, which extended the Zhao model to include a nonlocal spatial response to account for high spatial frequency cut-off – Model I [6]. A square root relationship, shown to exist between the polymerization rate and the illuminating intensity [7,8], was also incorporated – Model II [9]. Kinetics of the polymerization process have recently been examined [10,11] for the cases when the chain termination mechanism is either bimolecular (two chains terminating mutually) or primary (chain terminated with a free radical) – Model III. Renotte et *al*. [12] applied the NPDD model to successfully model higher harmonic grating components recorded in both polymer and polymer-dispersed liquid crystal based materials. The effects of shrinking and swelling play have also been examined and we outline a possible extension to the NPDD model, based on work by Sutherland et *al*. [13] to account for some of these effects. 3-D effects have also been examined [14,15] and shown to play an important role when recording gratings in thick polymer layers greater than 200μm. In this work we deal exclusively with layers of approximately 90μm and neglect 3-D effects.

In this paper we first extend Model II to include a nonlocal temporal response. The model is then solved using a Finite-Difference Time-Domain method (FDTD) [16]. We then examine the effects of the nonlocal temporal response on refractive index modulation using the Lorentz-Lorenz relation [17]. The diffraction efficiency of the resulting grating is calculated using Rigorous Coupled Wave Analysis (RCWA) [18] and we compare predictions to experimental results for both the primary and bimolecular cases.

2. Nonlocal polymerization-driven diffusion model, NPDD

The generalized 1-D NPDD partial differential equation describing photopolymerization in photopolymer can be written in the form:

$$\frac{\partial u(x,t)}{\partial t} = \frac{\partial}{\partial x}\left[D(x,t)\frac{\partial u(x,t)}{\partial x} \right] - \int_{-\infty}^{+\infty}\int_{0}^{t} R\left(x,x';t,t'\right) F\left(x',t'\right) \times \left[u\left(x',t'\right) \right]^{\beta} dt'dx' - \frac{u(x,t)}{u(x,t)+N(x,t)}\frac{\partial H(x,t)}{\partial t} \tag{1}$$

where $u(x, t)$ is the free-monomer concentration, $D(x, t)$ is the diffusion constant, $F(x, t)$ is the polymerization rate, $N(x, t)$ is the polymer concentration, $R(x, x'; t, t')$ is the nonlocal response function [6,9,19], $H(x, t)$ is the hole concentration and β is a factor introduced to specify the dominant chain termination mechanism, either bimolecular ($\beta = 1$) or primary ($\beta = 2$) [10,11].

If we assume that after a certain transience period the rate of hole creation will be approximately equal to the rate of hole collapse, $\partial H(h,t)/\partial t$ will be small and can be neglected from Eq. (1) [13]. The hole concept is useful in modelling the shrinkage associated with polymerization [20]. When polymerization takes place we say holes are generated which then collapse resulting in an overall reduction in volume. In this paper we assume that shrinkage and swelling effects are negligible.

The nonlocal response function represents the effect of polymer chain initiation at location x' and time t' on the amount of material being polymerized at location x and time t. Radical chain polymerization results in chain growth away from the point of initiation. The active tip of each chain combines with free monomer extending the polymer chain. This results in polymerization occurring nonlocal to the point of initiation as a function of both time and

space. In previous publications [3,4,9] it was assumed that following a brief transient period the spatial effect of chain growth was instantaneous (action-at-a-distance). However, where the use of short exposures is necessary, as in optical data storage, temporal effects become more significant. We now investigate the inclusion of a nonlocal temporal response.

2.1 Nonlocal Temporal Response

It is assumed that the nonlocal response function can be broken up into the product of a spatial and a temporal response, $R(x,x';\ t,t') = R(x,x')T(t,t')$. The purely temporal part of the response function takes account of the removal of monomer due to past initiations, over the time interval $0 \le t' < t$. In the local limit the time response function must have the following mathematical properties:

$$\lim_{T_{\max}\to 0}\left\{T\left(t',t\right)\right\} = \delta\left(t'-t\right), \tag{2a}$$

where $T_{\max}$ is defined as the maximum effective travel time between x and x' [6] and

$$\int_{-\infty}^{t} T\left(t',t\right)dt' = 1. \tag{2b}$$

Previously it is argued that only events in the recent past, quantified using $T_{\max}$, would give rise to significant nonlocal temporal effects and that at any time after $T_{\max}$ any change in monomer concentration at x' will give rise to an instantaneous change in the amount of polymerization at x. The time response must therefore have the property that

$$\int_{t-T_{MAX}}^{t} T\left(t',t\right)dt' \approx 1, \tag{3}$$

In this regime the material response function reduces to a purely spatial response. This assumption is clearly questionable at times close to zero before the average number of chains reaching a point has reached a steady state and it can be assumed that only slow adiabatic variations to the steady state occur with respect to time. In this paper we extend the nonlocal diffusion model to include both a nonlocal temporal and spatial response and examine the numerical results.

The contribution of a chain initiated at time t' and position x' to the polymer generated at time t and position x will decrease as the interval $t - t'$ increases. The biggest contribution to the removal of monomer at a point and time in space will be due to chains initiated at the same position and time. One possible temporal response function which satisfies Eqs. 2(a) and 2(b) is the area normalised exponential function,

$$T(t-t') = \frac{1}{\tau_n}\exp\left[\frac{\left(t-t'\right)}{\tau_n}\right]. \tag{4}$$

The time constant τ_n determines the extent of the nonlocal temporal response. As τ_n gets smaller the response becomes more localized and $T(t\text{-}t')$ approaches a delta function. The effects of introducing this nonlocal temporal response are discussed in Section 3.

3. Finite-difference method

Previously the NPDD model has been solved using a two or four-harmonic expansion [6,9]. Recently it has been shown that for certain parameter values a more rigorous method for solving the nonlocal diffusion equation is required. Wu and Glytsis [16] applied a finite-difference time-domain (FDTD) method to solve the NPDD model (Model II) in its

dimensionless form. In this paper we wish to extend this discussion to include nonlocal temporal effects.

(i) Firstly the nonlocal diffusion equation is rewritten in the dimensionless form:

$$\frac{\partial u(x_D,t_D)}{\partial t_D} = R_D \frac{\partial}{\partial x_D}\left[D_D(x_D,t_D)\frac{\partial u(x_D,t_D)}{\partial x_D}\right] - \int_{-\infty}^{+\infty}\int_0^t R\left(x_D,x_D';t_D,t_D'\right)F\left(x_D',t_D'\right)u\left(x_D',t_D'\right)dt_D'dx_D' \tag{5}$$

where $x_D = Kx$, $t_D = F_0 t$, R_D is the dimensionless reaction rate where $R_D = DK^2/F_0$ and $K = 2\pi/\Lambda$ where Λ is the exposing pattern period. $F_0 = \kappa I_0 t$, where κ is the polymerization constant and I_0 is the average exposure intensity. Combining a nonlocal Gaussian spatial response and the nonlocal exponential temporal response

$$R\left(x_D,x_D';t_D,t_D'\right) = \frac{1}{\sqrt{2\pi\sigma_D}}\exp\left[\frac{-\left(x_D-x_D'\right)^2}{2\sigma_D}\right]\times\frac{1}{\tau_{nD}}\exp\left[\frac{\left(t_D-t_D'\right)}{\tau_{nD}}\right], \tag{6}$$

where σ_D and τ_{nD} are the normalized nonlocal parameters.

(ii) Secondly we discretize the diffusion equation in dimensionless space. A Taylor series expansion of $u(x_D,t_D)$ around a given point x_D gives

$$\frac{\partial u_i}{\partial x_D} \cong \frac{1}{2\Delta x}\left(u_{j+1}-u_{j-1}\right) \tag{7a}$$

and

$$\frac{\partial^2 u_i}{\partial x^2{}_D} \cong \frac{1}{\Delta x^2}\left(u_{i+1}-2u_i+u_{i-1}\right), \tag{7b}$$

where u_i is the monomer concentration at ith dimensionless-space point and Δx is the dimensionless space increment.

(iii) Thirdly the diffusion equation is discretised in dimensionless time. Again a Taylor series expansion of $u(x_D,t_D)$ around a given time t_D gives

$$\frac{\partial u_j}{\partial t_D} \cong \frac{u_{j+1}-u_j}{\Delta t_D}, \tag{7c}$$

where u_j is the monomer concentration at the jth dimensionless-time step and Δt_D is the dimensionless time increment. Substituting Eqs. (6) and (7) into Eq. (5) we can write an expression for monomer concentration as

$$\begin{aligned} u(i,j) \cong & \left[1-2C_2(i,j-1)\frac{\Delta t_D}{\Delta x_D{}^2}\right]u(i,j-1) \\ & +\left[C_2(i,j-1)\frac{\Delta t_D}{\Delta x_D{}^2}+C_1(i,j-1)\frac{\Delta t_D}{\Delta x_D{}^2}\right]u(i+1,j-1) \\ & +\left[C_2(i,j-1)\frac{\Delta t_D}{\Delta x_D{}^2}-C_1(i,j-1)\frac{\Delta t_D}{\Delta x_D{}^2}\right]u(i-1,j-1)-\Delta t_D C_3(i,j-1), \end{aligned}$$

(8)

where

$$C_1(i, j-1) = R_D \frac{\partial D_D\left(x_{D,i}, t_{D,j-1}\right)}{\partial x_D}, \tag{9a}$$

$$C_2(i, j-1) = R_D D_D\left(x_{D,i}, t_{D,j-1}\right), \tag{9b}$$

$$C_3(i, j-1) = \frac{\Delta x_D}{2}\left[f_D(1, j-1) + 2\sum_{k=2}^{N-1} f_D(k, j-1) + f_D(N, j-1) \right] \tag{9c}$$

and

$$f_D(k, j-1) = R\left(x_{D,i}, x_{D,k}\right)\ F\left(x_{D,k}\right)\ u\left(x_{D,k}, t_{D,j-1}\right). \tag{9d}$$

N is the number of sampling points in the dimensionless-space domain and $\Delta x_D = 2\pi/(N-1)$. For numerical stability the increment in the dimensionless-time domain, Δt_D, must satisfy the stability criterion [16]

$$\Delta t_D \le \frac{1}{2}\frac{{\Delta x_D}^2}{R_D}. \tag{10a}$$

In most cases we choose $\Delta t_D = 0.4\ (\Delta x_D{}^2/R_D)$, which is consistent with the Wu and Glytsis analysis [16]. However the diffusion model now includes a time integral. In evaluating this integral, using the trapezoidal rule, the size of Δt_D is critical to the numerical accuracy of the result. To estimate a suitable value of Δt_D in this case we examine the truncation error associated with the trapezoidal rule. Using the Taylor series it can be shown that the modulus of the truncation error, $|e|$, for the integral, $\int_0^{t_D'} T\left(t_D, t_D'\right) dt_D$, is given by [21]

$$|e| \le \frac{1}{12}{\Delta t_D}^2 \left|T''(\tau)\right| \times t_D \tag{10b}$$

where $\left|T''(\tau)\right| = \max\left\{ \left|T\left(x, t_D'\right)\right| \ ;\ 0 \le x \le t_D' \right\}$.

By choosing a suitable value for the maximum allowable truncation error in our system we can then estimate an appropriate value for Δt_D. The truncation error used was $|e| = 0.005$. The polymer concentration at the ith dimensionless-space point can then be determined by the equation

$$N(i, j) \cong \frac{\Delta t_D}{2}\left[C_3(i, 0) + 2\sum_{k=1}^{j-1} C_3(i, k) + C_3(i, j) \right]. \tag{11}$$

The time evolution of the harmonic components of the polymer grating profile is found by applying the discrete Fourier transform to the resulting data at each time step.

3.1 Numerical Results

We examine the nonlocal model for different values of the nonlocal response parameter. Simulations of the numerical model are carried out for different combinations of values of τ_{nD} (0.01, 0.05, 0.1) to investigate the effect of the inclusion of the nonlocal temporal response on the evolution of the harmonic coefficient amplitude. In all of the simulations we choose R = 50, corresponding to a relatively high fidelity material, γ= ½, corresponding to a non-linear material and β = 1, corresponding to a material where bimolecular chain termination is dominant. The results are shown in figure 1. N_0, N_1, N_2, N_3, correspond to the amplitudes of the first four harmonics that make up the grating profile. High fidelity materials will exhibit high first harmonic, N_1, values and low higher hamonic values, which in our model correspondes to a material with a high R value ($R \approx 50$). Conversely low fidelity materials will have lower N_1 values and larger higher harmonic components, corresponding to a low R value ($R \approx 0.1$). We see in figure 1 that the saturation values of each harmonic for the three values of τ_{nD} are almost identical. However the form of the harmonic time evolution during the early stages of grating growth is clearly affected.

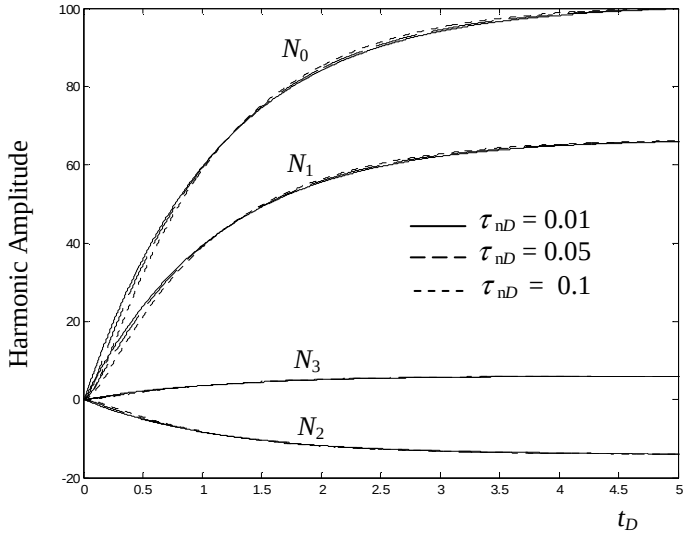

Fig. 1. Harmonic coefficient amplitudes of polymer concentration for values of nonlocal temporal response parameter τ_{nD} = (0.01, 0.05, 0.1), where R_D = 50, σ_D = 0 and β = 1.

As the value of τ_{nD} increases, the extent of the nonlocal temporal response increases and the initial rate of grating gowth decreases. This illustrates the existence of a transient period in the early stages of grating evolution. In the next section we investigate the effects of the nonlocal temporal response if illumination is stopped during the recording process prior to reaching saturation.

4. Chain growth after illumination: dark reactions

In previous papers [4-6] it was assumed that rate of polymerization responded instantaneously to changes in light intensity, i.e. there is no temporal response. Therefore if illumination stopped during grating formation, polymerization stopped instantaneously. Based on the above analysis, and assuming that all the monomer has not been consumed completely by the end of illumination, we would expect initiated chains to continue growing after for some short time after exposure before terminating. Colvin et *al*. [22] examined the harmonic evolution of polymer after exposure. However any subsequent change in the harmonic amplitude was

attributed solely to monomer diffusion. The effects of "dark reactions", i.e. continued polymer growth after illumination, were ignored. In this section we examine the effects of the inclusion of a nonlocal temporal response on harmonic evolution when illumination is stopped during recording. Then in Section 5 we include the effects of monomer diffusion.

4.1 Simulation results

Simulations were carried out for short exposures using the finite difference method as described in Section 3. Illumination was stopped after t_D = 0.1 by setting the exposing intensity to zero after this point. Different values of the nonlocal temporal response parameter τ_{nD} are used in each simulation as shown in figure 2.

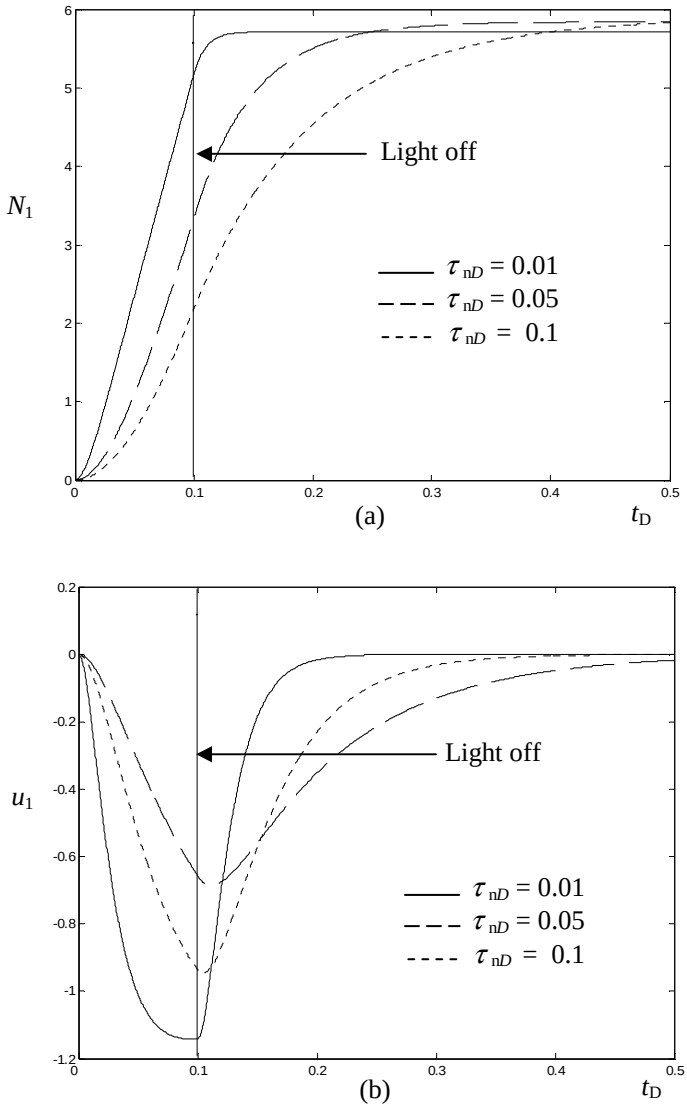

Fig. 2. (a) Polymer and (b) Monomer harmonic amplitudes for τ_{nD} = (0.01, 0.05, 0.1) where R_D=50, σ_D = 0, α = 0, γ = 1/2 and β = 1.

In each case the evolution of the monomer and polymer harmonics was examined. Figures 2 (a) and (b) show the first harmonic component of polymer and monomer respectively for three different values of τ_{nD}. For the smaller values of τ_{nD} we see that there is little increase in N_1, polymer harmonic amplitude, after exposure has stopped. However as the value of τ_{nD} increases the amplitude of the polymer harmonic continues to increase significantly before reaching its maximum value. Similarly the monomer harmonic amplitude decreases as the monomer diffuses back into the depleted regions of the grating layer. Assuming chain termination is not instantaneous once exposure has stopped, and based on the above simulation, we see continued polymerization for a short period after exposure. In the next section we examine the evolution of the resulting refractive index modulation based on the above simulations.

5. Refractive index modulation evolution

In this section we first report our experimental and theoretical work to estimate the refractive index of the main components of the photopolymer recording material. We then discuss the significance of these refractive index values on the time evolution of the refractive index modulation and on the diffraction efficiency of the grating.

5.1 Refractive index measurements

The unpolymerized acrylamide-based photopolymer holographic recording material used is made up of a monomer, Acrylamide; a binder, Polyvinylalcohol (PVA); a crosslinker, Bisacrylamide; a dye, Erythrosine B and an electron donor, TEA [4].

Table 1. Concentrations and volume fractions of photopolymer material components.

Component	Mass (grams)	Density (g/cm^3)	Volume (cm^3)	Volume Fraction
PVA	7	1.3	5.384615	0.333025
Acrylamide	2.4	1.122	2.139037	0.132294
Bisacrylamide	0.8	1.24	0.645161	0.039902
TEA	8.992	1.124	8	0.49478

A Metricon 2010 Prism Coupler [23] in Thick Film / Bulk material index mode was used to perform the refractive index measurements reported here. Solution containing different combinations of material components were prepared and then allowed to dry on glass slides. The refractive indices of the layers were then measured at a wavelength of 633 nm. The results are given in Table 2.

Table 2. Refractive index measurements of material components.

Material composition	Refractive index measured
PVA	1.5127
PVA + TEA	1.4957
PVA + TEA + DYE	1.4965
PVA + TEA + Acrylamide	1.4924
PVA + TEA + Acrylamide + Dye	1.4941
PVA + TEA + Acrylamide + Bisacrylamide	1.4948

The average refractive index of the material is dependent upon the refractive index of the individual material components and their concentrations or volume fractions. This relationship can be expressed using the Lorentz-Lorenz relation [17]:

$$\frac{n^2-1}{n^2+2}=\phi^{(m)}\frac{{n_m}^2-1}{{n_m}^2+2}+\phi^{(p)}\frac{{n_p}^2-1}{{n_p}^2+2}+\phi^{(b)}\frac{{n_b}^2-1}{{n_b}^2+2}. \tag{12}$$

n_{m}, n_{p} and n_{b} are the refractive indices of monomer, polyacrylamide and some background material respectively and $\phi^{(m)},\phi^{(p)}$ and $\phi^{(b)}$ are the respective volume fractions of these components where the volume fraction is given by $\phi_i = x_i v_i \Big/ \sum_i x_i v_i$, where x_i is the mole fraction and v_i is the molar volume of the i^{th} component. The material is therefore made up mainly of monomer, polymer and a background material (PVA + TEA) and we assume that the total volume fraction is approximately conserved during short exposures [17,22] i.e.

$$\phi^{(m)}+\phi^{(p)}+\phi^{(b)}+\phi^{(h)}=1, \tag{13}$$

where $\phi^{(h)}$ is the hole volume fraction. We assume $\phi^{(h)}$ to be very small and therefore it can be neglected [24]. The effect of holes is briefly discussed later in Section 7. Combining the data from Tables 1 and 2 and applying the Lorentz-Lorenz relation, refractive index values for the main components of the material were estimated. The results are shown in the Table 3.

Table 3. Refractive index values of material components found in the literarure and those calculated from the results in table 2 in conjunction with the Lorentz-Lorenz relation.

Chemical	**Refractive index , $n^{\mathrm{literature}}$**	**Refractive index , $n^{\mathrm{calculated}}$**
PVA	1.52-1.55 [25]	1.5127
TEA	1.485 [26]	1.48446
Acrylamide	n_x = 1.46, n_y = 1.55, n_z = 1.581 [27]	1.47162

The estimated values of refractive index for PVA and TEA agree closely with those in the literature. Independent verification of our refractive index value for Acrylamide is less clear as it is dependent on the form of the material. However having used the same method to calculate the refractive index for the previous two components, we believe our result is consistent. We note that the refractive index values have been estimated based on measurements of dry layers at 633 nm, which replicates experimental grating analysis conditions. The values presented in Table 3 are now substituted into our model to examine the temporal evolution of the refractive index modulation during and immediately after the formation of transmission holographic gratings in our photopolymer.

5.2 Refractive index modulation and diffraction efficiency

Using Eq. 12 and following the analysis by Aubrecht et *al*., [17] with a minor typographical correction (6 appears in the denominator of the first part of the right hand side of the equation instead of 3) the refractive index modulation can be written as

$$n_1=\frac{\left(n_{\mathrm{dark}}^2+2\right)^2}{6n_{\mathrm{dark}}}\left[\phi_1^{(m)}\left(\frac{{n_m}^2-1}{{n_m}^2+2}-\frac{{n_b}^2-1}{{n_b}^2+2}\right)+\phi_1^{(p)}\left(\frac{{n_p}^2-1}{{n_p}^2+2}-\frac{{n_b}^2-1}{{n_b}^2+2}\right)\right], \tag{14}$$

where n_{dark} is the refractive of the material before exposure. $\phi_1^{(m)}$ and $\phi_1^{(p)}$ are the first harmonic volume fraction components of monomer and polymer respectively. The refractive index values for monomer and binder are as given in Table 1. We can then estimate n_{dark} using Eq. 14 where the initial volume fraction of monomer, $\phi_1^{(m)}$, was calculated to be 0.13 (see Table 1). This gives $n_{dark} \approx 1.49$. Using Eq. 13 and the harmonic values determined in Section 4 we now examine the evolution of the refractive index modulation.

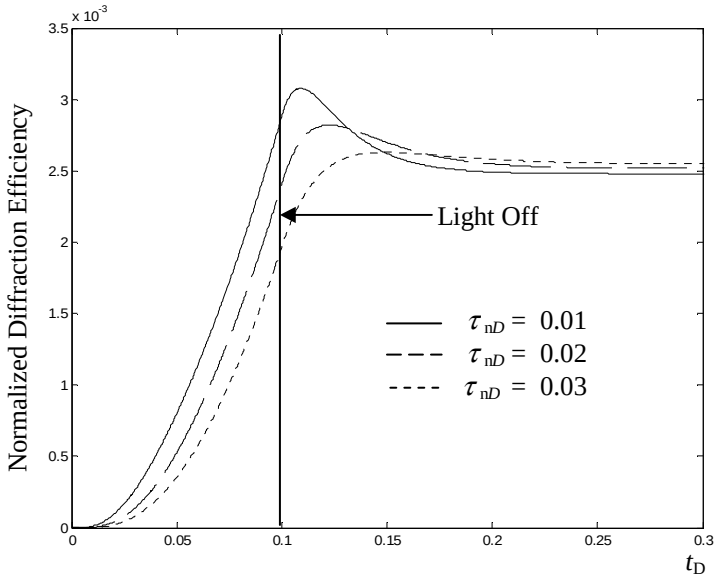

Fig. 3. Theoretical refractive index evolution where R_D=50, $\sigma_D = 0$, $\alpha = 0$ and $\beta = 1$.

Figure 3 shows a plot of diffraction efficiency (where the definition of diffraction efficiency is as defined by Moharam and Gaylord [18]), calculated from the corresponding refractive index modulation values using RCWA [18]. 21 harmonics are retained in the RCWA for TE polarization and a material thickness of 90μm. As expected from our analysis in Section 4, based on the NPDD model with nonlocal temporal response, the refractive diffraction continues to increase after the exposure ends. Now, however, we also take into account the effect of monomer diffusion after exposure. The values estimated for the refractive index of the monomer and background demonstrate that $n_b > n_m$. Therefore as the monomer continues to diffuse back into the polymerized regions post exposure the refractive index in these regions is reduced and hence the refractive index modulation decreases.

6. Experimental results

The photopolymer solution is deposited on glass slides [28] allowed to dry for 48 hours. The resulting dry layers have a thickness of 90 ± 5 μm. Transmission holographic gratings were recorded with a spatial frequency of 1000 lines/mm. Recording was carried out using a 532 nm solid-state laser type with a recording intensity of 2 mW/cm^2. During and post exposure a 633 nm HeNe laser was used to monitor the evolution of the grating diffraction efficiency. Short exposure experiments were carried out, each for a different exposure time. The exposure time is controlled using a shutter which closes after the required recording time. The diffraction efficiency was monitored for some time after this point. Diffraction efficiency values are then suitably corrected for Fresnel reflections. Typical results are shown in figure 4. We note a dead band region determined to be ~ 0.2 seconds, at the start of the recording process. This is due to the induction period associated with the excitement of the

dye and the initiation of chains and also due to inhibition of chain initiation most probably due to oxygen [29,30].

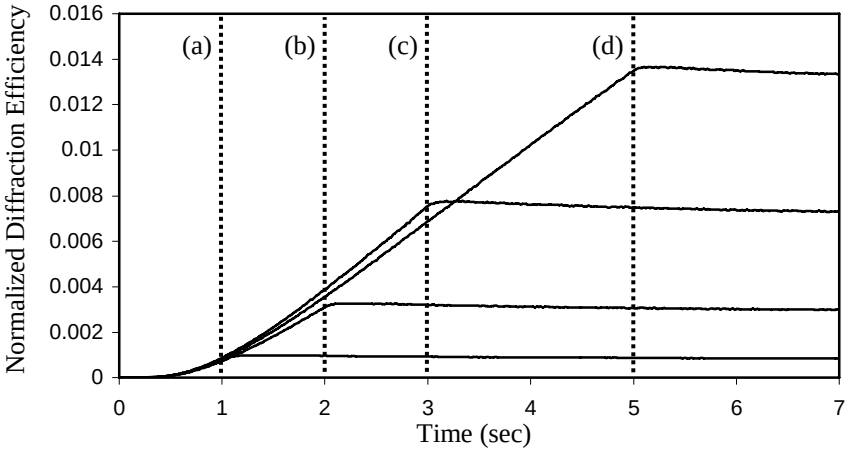

Fig. 4. Diffraction efficiency evolution for short exposures. Exposure times are 1, 2, 3 and 5 seconds for (a), (b), (c) and (d) respectively.

From the results shown in figure 4 we can see a slight rapid increase in diffraction efficiency after exposure ends followed by a slower decrease before stabilizing. These results follow the diffraction efficiency evolution predicted by the theoretical simulations presented in Sections 4 and 5 based on the independently determined refractive index measurements described in Section 5. Therefore the experimental results would appear to confirm that a continued diffraction efficiency growth increase takes place after exposure arising due to chain growth and the subsequent decrease can be attributed to slower monomer diffusion. In the next section, by fitting experimental results, material parameters are estimated and our model further validated.

6.1 Least square fitting

A nonlinear fitting algorithm is used in conjunction with the NPDD for both the bimolecular ($\beta = 1$) and the primary case ($\beta = 2$). To proceed, starting values and sensible ranges over which our fitting algorithm can search must be first determined. It is important to note that some parameter units change when going from the bimolecular model to the primary model. Where confusion may occur we differentiate between the two models using the superscript II for model II, bimolecular termination and the superscript III for model III, primary termination [10]. Based on previous fits to experimental data [10] we expect, for $\beta = 1$ (bimolecular), an R value within the range $1 \leq R^{II} \leq 12$ and for $\beta = 2$ (primary), an R value within the range $50 \leq R^{III} \leq 115$ (mol/cm^3). To reduce the number of fitting variables and thus simplify our task, we assume a κ^{II} value of 0.05 $s^{-1}mW^{-1/2}cm$ for $\beta = 1$ and a κ^{III} value of 0.00036 $s^{-1}mW^{-1/2}cm^4mol^{-1}$ for $\beta = 2$ and a nonlocal spatial response length of $\sqrt{\sigma'}$ = 60nm in each case. These values are used as they are typical of values experimentally determined in previous work [10]. The refractive index values are allowed to vary by ± 0.02 from the values which have been experimentally determined and given in Section 5, Table 3. As mentioned in the first part of this section, a dead band region exists at the beginning of the recording process. This is neglected during the fitting process.

Based on these values we determine the evolution of the refractive index modulation. This is then converted to diffraction efficiency values using the RCW model and the results fitted to the experimental data. Fitting is carried out in Matlab [31] using a non-linear Gauss-Newton based algorithm. The algorithm attempts to minimise the error function,

$\frac{1}{2}|F(x, xdata) - ydata|^2$, where $ydata$ is the experimentally determined diffraction efficiency and $F(x, xdata)$ is the theoretical prediction returned by the nonlocal model. The mean square error (MSE) values determined for each fit are given in Tables 4 and 5. Fitting is carried out for both the primary and bimolecular termination based NPDD models. The results are given below with the error bars reflecting uncertainties of ± 5% associated with the reproducibility of the measurements themselves.

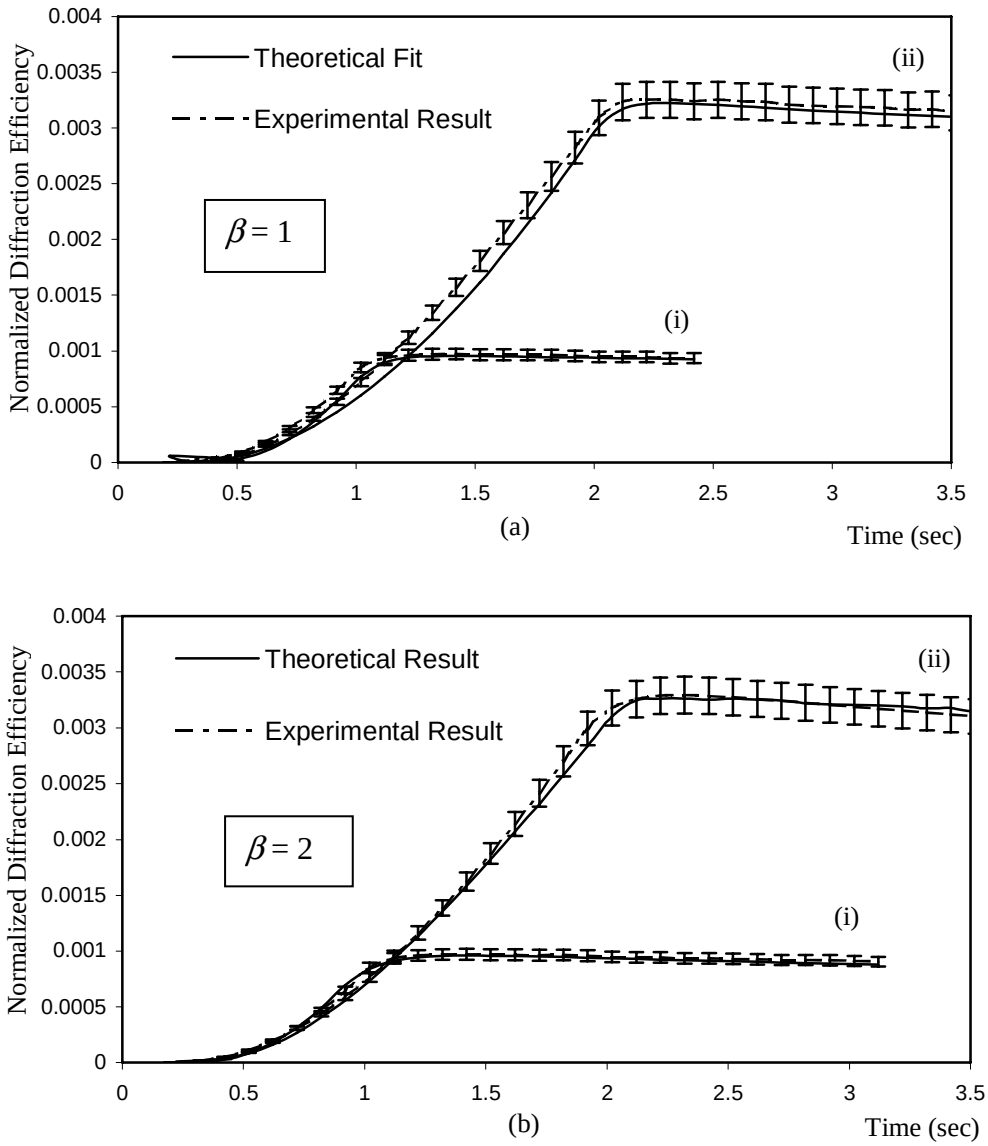

Fig. 5. Fit to experimental data using (a) the bimolecular termination model and (b) the primary termination model where the parameter values used are those given in Tables 4 and 5 for (i) 1 and (ii) 2 second exposures.

Figure 5 shows fits to experimental data for (a) the bimolecular and (b) the primary termination chain termination case. The best-fit parameter values are shown in Tables 4 and 5 below.

Table 4. Best fit parameters obtained for the ideal case of bimolecular termination, $\beta = 1$.

Exposure Time (sec)	$n_{\text{polyacryl.}}$	$n_{\text{back.}}$	$n_{\text{acryl.}}$	τ_n **(sec)**	$\sqrt{\sigma'}$ **(nm)**	R	D **(cm^2/s) (x 10^{-10})**	**MSE (x 10^{-9})**
1	1.5101	1.495	1.493	0.09	60	8	2	2.1
2	1.5061	1.494	1.493	0.09	60	8	2	9.3

Good consistent fits are achieved for $\beta = 1$ in both exposure times. However there is a difference 0f 1.5% between the independently determined value of $n_{\text{acrylamide}}$, 1.471 and the fit value, 1.493. The monomer diffusion value is within the range expected for this type of material where D can range from 10^{-14} cm^2 s^{-1} for highly viscous systems to 10^{-8} cm^2 s^{-1} for very fluid systems [32].

Table 5. Best fit parameters obtained for the non-ideal case of primary termination, $\beta = 2$.

Exposure Time (sec)	$n_{\text{polyacryl.}}$	$n_{\text{back.}}$	$n_{\text{acryl.}}$	τ_n **(sec)**	$\sqrt{\sigma'}$ **(nm)**	R **(mol/cm^3)**	D **(cm^2/s) (x 10^{-11})**	**MSE (x 10^{-10})**
1	1.502	1.495	1.48	0.12	60	100	1.8	3.9
2	1.5	1.494	1.48	0.13	60	80	1.4	25

Fits for the primary case, to the same data sets, are shown in Figure 5b. The corresponding parameter values are given in Table 5. The error between the experimental and theoretical data is noticeably less than that for the bimolecular case with the best-fit value for $n_{\text{acrylamide}}$ being 1.48 and the independently determined value of 1.471, the difference being only 0.6%. The value for the diffusion constant of monomer, $D = 1.6 \pm 0.2\ 10^{-11}$ cm^2 s^{-1} is within the range expected and similar to values reported in the literature for similar types of material [10,16,33]. The nonlocal response time constants are of the order of 10^{-1}s which seem reasonable in light of the brief transient periods observed at the start and end of the exposure.

7. Discussion and conclusion

In this paper we have:

(i) Investigated the effect of including a nonlocal temporal response in the NPDD model. Numerical results have shown that as the extent of the nonlocal temporal response changes, the evolution of the polymer harmonics during the initial stages of exposure also change.

(ii) Examined the effect of the inclusion of the temporal response when modelling grating evolution after exposure has stopped. Based on the assumption that chain termination is not instantaneous, numerical simulations predict continued polymerization for a brief period after exposure ends.

(iii) Estimated the refractive index of the main components of the photopolymer recording material. Based on these and combining the nonlocal diffusion model and the appropriate Lorentz-Lorenz relations we have examined the evolution of the refractive index modulation during short exposures and also immediately post illumination. It has been shown that with the inclusion of a nonlocal temporal response, the refractive index modulation continues to increase after illumination and then decreases as the amplitude of the monomer grating decreases due to monomer diffusion.

(iv) Fit experimental results using the NPDD model and RCW analysis for both the bimolecular and primary termination models. Good fits are achieved in both cases. However better fits are achieved for the primary case, indicating that primary termination may be the more dominant termination mechanism for short exposures. We note that this supports our previously reported results [10].

(v) We have: provided further evidence that the NPDD mode, with the inclusion of a nonlocal temporal response and based on independently determined refractive index values, can be used to accurately predict the nature of grating evolution in acrylamide based photopolymers.

We note that much remains to be done. The collapse of holes, left as a result of conversion of monomer into polymer will lead to an increase in density due to shrinkage. We note that any such shrinkage will occur in the areas of high polymerization and will lead to higher refractive index modulation. Time lags associate with hole collapse might therefore be expected to vary the diffraction efficiency post exposure. However we do believe that the assumption to ignore shrinkage is valid in this paper where very small volumes of polymer are generated during the brief recording periods. We further note that swelling due to environmental effects such as humidity will also change post exposure behavior [20]. Future work must also include modelling of the dead band and inhibition effects noted during grating recording [29,30].

Acknowledgments

We acknowledge the support of Enterprise Ireland and Science Foundation Ireland through the through the Research Innovation Fund, the Basic Research Program and the Research Frontiers Program and of the Irish Research Council for Science, Engineering and Technology.